doi:10.26443/seismica.v4i2.1418

Investigating the D” Reflector Beneath the Indian Ocean with Source Arrays

C. Thomas *[1,2], **B.H. Heyn** [3], **L.S. Tölle** [1], **R. van Tent** [1]

[1]Institute of Geophysics, University of Münster, Germany, [2]Geological Survey of Denmark and Greenland, Copenhagen, Denmark, [3]Centre for Planetary Habitability (PHAB), Department of Geosciences, University of Oslo, Norway

Author contributions: *Conceptualization*: C. Thomas. *Formal Analysis*: C. Thomas, B.H. Heyn, L.S. Tölle,. *Funding Acquisition*: C. Thomas. *Investigation*: C. Thomas, B.H. Heyn. *Methodology*: C. Thomas, B.H. Heyn. *Supervision*: C. Thomas. *Validation*: C. Thomas, B.H. Heyn, R.van Tent. *Visualization*: C. Thomas, B.H. Heyn. *Writing – original draft*: C. Thomas. *Writing – review & editing*: C. Thomas, B.H. Heyn.

Abstract We used seismic P-wave reflections to search for the discontinuity at the top of the D” region beneath the Indian Ocean. Due to a lack of seismic receiver arrays to target this region, we build source arrays using earthquakes in Indonesia and taking advantage of the long-running history of GEOSCOPE stations located in the western Indian Ocean and Antarctica, as well as three additional stations (Seychelles and Antarctica). Despite restricting the earthquake depth range, source-array stacks were difficult to interpret due to complications arising from differing earthquake depths, violating the plane wave assumption. Therefore, we use a source-array scatter imaging method, that does not rely on travel-times calculated for a plane wave. Using this technique in conjunction with source normalization, we found evidence for a D” P-wave reflector for several stations with reflector depths varying between 230-160 km above the CMB South of Australia and 190 to 270 km above the CMB beneath the Indian Ocean, where the depth of the reflector in the north of our study area is consistent with previously imaged D” depths using S-waves and agrees with receiver array data. We suggest that earlier imaged subducted lithosphere in this region is responsible for our D” reflections.

Production Editor:
Yen Joe Tan
Handling Editor:
Lauren Waszek
Copy & Layout Editor:
Hannah F. Mark

Received:
July 25, 2024
Accepted:
June 6, 2025
Published:
July 8, 2025

Non-technical summary When imaging the reflector at the top of the D” region in the Earth's lowermost mantle, it is common to use receiver arrays (one source, several receivers). However, some regions cannot be sampled this way because suitable seismic arrays are scarce. In these cases, it is possible to use several earthquakes recorded at one station, thereby building a source array. Due to the different depth of earthquakes, stacking techniques, that rely on pre-calculated travel times for a single event to a number of stations located at the surface, are difficult to use and the reflections are barely visible. Here, we focus on a method, which we call source migration, that uses travel times calculated for each earthquake separately before stacking the data. We show that we are able to detect a seismic reflector in a region where previously, using tomographic inversions, subducted lithosphere was imaged in the Indian Ocean close to the core-mantle boundary. Our results show a reflector, likely due to this subducted lithosphere, that thins from the north to the south. The reflector depth in the northern part of our study region, using P-waves, agrees with previous results using receiver-array S-wave reflections.

1 Introduction

The lowermost 200 to 300 km of the mantle, also called the D” region (Bullen, 1950), exhibits seismic structures with a range of different length scales: small-scale scatterers (e.g., Mancinelli et al., 2016; Hedlin and Shearer, 2000; Haddon and Cleary, 1974) and ultra-low velocity zones (Yu and Garnero, 2018), with length scales of 10s of kilometers, up to large-scale structures, such as a reflector at the top of the D” region (see reviews by Lay, 2015; Cobden et al., 2015; Wysession et al., 1998) and large low seismic velocity provinces (reviews by Garnero et al., 2016; McNamara, 2019; Koelemeijer, 2021), with dimensions of hundreds to thousands of kilometers. These structures are related to the interaction of mantle dynamics and the mineralogy of the deep Earth. Many different approaches have been undertaken to understand the nature of these structures, using a variety of methods, and spanning the fields of seismology, mineral physics, and geodynamics.

Due to limited station coverage and arrays in ocean basins and portions of the southern hemisphere (e.g., Lay et al., 2002; Simmons et al., 2015; Ringler et al., 2022), some areas of the lowermost mantle are difficult to investigate with seismology. One example is the lowermost mantle beneath the Indian Ocean. Although a recent, global body-wave tomography study (Simmons et al., 2015) indicates that ancient subducted lithosphere reached the base of the mantle west of Australia, this slab has not been previously observed in reflection data. The region is adjacent to a large area with reduced seismic velocities beneath Africa (e.g., Ritsema et al., 2010), and long-lived volcanism is found in the Indian Ocean (e.g., La Réunion, Seychelles, Mauritius), which is attributed to a lowermost mantle source

*Corresponding author: cthom_01@uni-muenster.de

at the edge of the African LLSVP (e.g., Tsekhmistrenko et al., 2021). In addition, the largest geoid anomaly on Earth, located beneath the southern tip of India, may be caused by the combination of a lower mantle slab (such as the one imaged by Simmons et al., 2015) and an upwelling, whose top is currently situated in the mid-mantle, but which may originate in the lower mantle (e.g., Reiss et al., 2017; Spasojevic et al., 2010; Greff-Lefftz et al., 2016). All of these aspects show the complexity of the region and detailed imaging of the lowermost mantle beneath the Indian Ocean could provide a better understanding of the dynamics and mineralogy in this region. For this, especially observations of P- and S-wave D" structure as well as anisotropy in D" would provide useful insights (e.g., Pisconti et al., 2022), but are currently unavailable for this area.

Here we concentrate on the reflector at the top of the D" region, which has been identified in many different places around the world. Seismic arrivals between the direct P- (or S-) wave and the core-mantle boundary (CMB) reflection, PcP (or ScS), have been detected in many regions since the publications by Lay and Helmberger (1983) and Wright et al. (1985). Based on the slowness (move-out) of the PdP arrival (Figure 1a) between P and PcP (or SdS between S and ScS), the wave has been identified as a reflection at a seismic discontinuity (D") a few hundred km above the CMB, which is often associated with the top of subducted lithosphere near the CMB (e.g., Lay and Helmberger, 1983; Weber, 1993; Wysession et al., 1998; Cobden et al., 2015; Lay, 2015; Jackson and Thomas, 2021) or the phase transition to post-perovskite in colder than average regions (e.g., Lay, 2015; Cobden et al., 2015). As shown in Figure 1a, the wave we call PdP in the following is a combination of the D" reflection, PdP (or SdS), and the diving wave, PDP (or SDS). Since the D" reflection is often small in amplitude, especially compared to P-waves, seismic array methods (Rost and Thomas, 2002; Schweitzer et al., 2009) help to enhance the small-amplitude signal while also allowing the slowness of the waves to be determined, thereby aiding in D" reflector identification (e.g., Weber, 1993; Cobden et al., 2015).

Previous studies (Young and Lay, 1987; Kendall and Shearer, 1994) using S-wave reflections from the top of the D" layer have examined the northern part of the Indian Ocean, and Young and Lay (1987) found evidence for an S-wave velocity increase of 2.7% approximately 280 km above the CMB. However, their study did not use P-wave reflections, and it did not extend further south where the tomographic inversion of Simmons et al. (2015) showed evidence for subducted lithosphere residing at the CMB. Wright and Kuo (2007), on the other hand, used P-waves with large epicentral distances to map the western part of the Indian Ocean and they found evidence for a discontinuity around 210 km above the CMB with a small velocity contrast. Here, we aim to use P-waves and illuminate regions further south compared to those imaged by Young and Lay (1987), and further east, compared with Wright and Kuo (2007). We investigate the deep mantle close to the area where Simmons et al. (2015) imaged high velocities in the lowermost mantle. Other tomographic images (compare e.g., models provided in Submachine, Hosseini et al., 2018) show a varied picture of fast and slow velocity anomalies in the lower mantle beneath this region, possibly due to a lack of seismic data, or because a number of different structures with different seismic velocities that are found close to each other. A confirmation of a reflector with a velocity increase at the top of D" near the CMB in this region would therefore help to confirm the presence of deep subducted lithosphere.

In the past, seismic observations recorded by networks or small-aperture seismic arrays have been used to identify the D" reflection, making use of its different move-out or slowness (and therefore its different incidence angle at the array) compared to the main phases and the CMB reflections (Figure 1). As some regions lack suitable source-receiver array combinations, the concept of source arrays has been developed (e.g., Krüger et al., 1995), which relies on a number of sources in a given area recorded at a single station (Figure 1b). However, this method has mostly been used in combination with receiver arrays for double-array stacks, or double beam-forming, in regions with large data availability (e.g., Krüger et al., 1995; Scherbaum et al., 1997; Yamada and Nakanishi, 1996; Reasoner and Revenaugh, 1999; Kito and Krüger, 2001; Kito et al., 2004; Thomas et al., 2002), and this approach is therefore still limited to areas where receiver array data can be obtained. Source arrays alone have mostly been used with nuclear explosions (e.g., Krüger et al., 1995) and we build upon this approach here, but we use source arrays (Figure 1b) with real earthquakes and stations from the GEOSCOPE network (e.g., Romanowicz et al., 1984; Roult et al., 2010; Douet et al., 2016) that provide the unique opportunity to sample areas of the deep mantle beneath the Indian Ocean. We complement our dataset with stations located in Antarctica and on the Seychelles that have been recording for a long time period. We aim to test whether source arrays could potentially be used to image the D" beneath this region, if the events are limited in focal depth range and have longer periods (2-5s) as opposed to short period (1Hz) nuclear explosion data (Krüger et al., 1995), and short-period filtered P-wave reflections off the top of D" (e.g., Weber, 1993; Thomas and Weber, 1997). However, since events within the source arrays are likely to have different focal mechanisms and waveforms, the seismic traces have to be corrected for their respective source time function before stacking. In this study, we test a range of source normalization methods to assess whether different approaches can improve waveform stacks. We also extend our approach to include a scatter imaging method: a simplified time migration method, that potentially allows us to find the depth of structures in the lowermost mantle (e.g., Thomas et al., 2004a,b).

2 Data set and source arrays

Since we are interested in mapping the D" layer in a region that is difficult to sample with receiver arrays, we focus on source arrays (Figure 1b), using single stations in the Indian Ocean (namely, stations RER, PAF, AIS, CRZF, MSEY and FOMA) as well as stations DRV, MAW

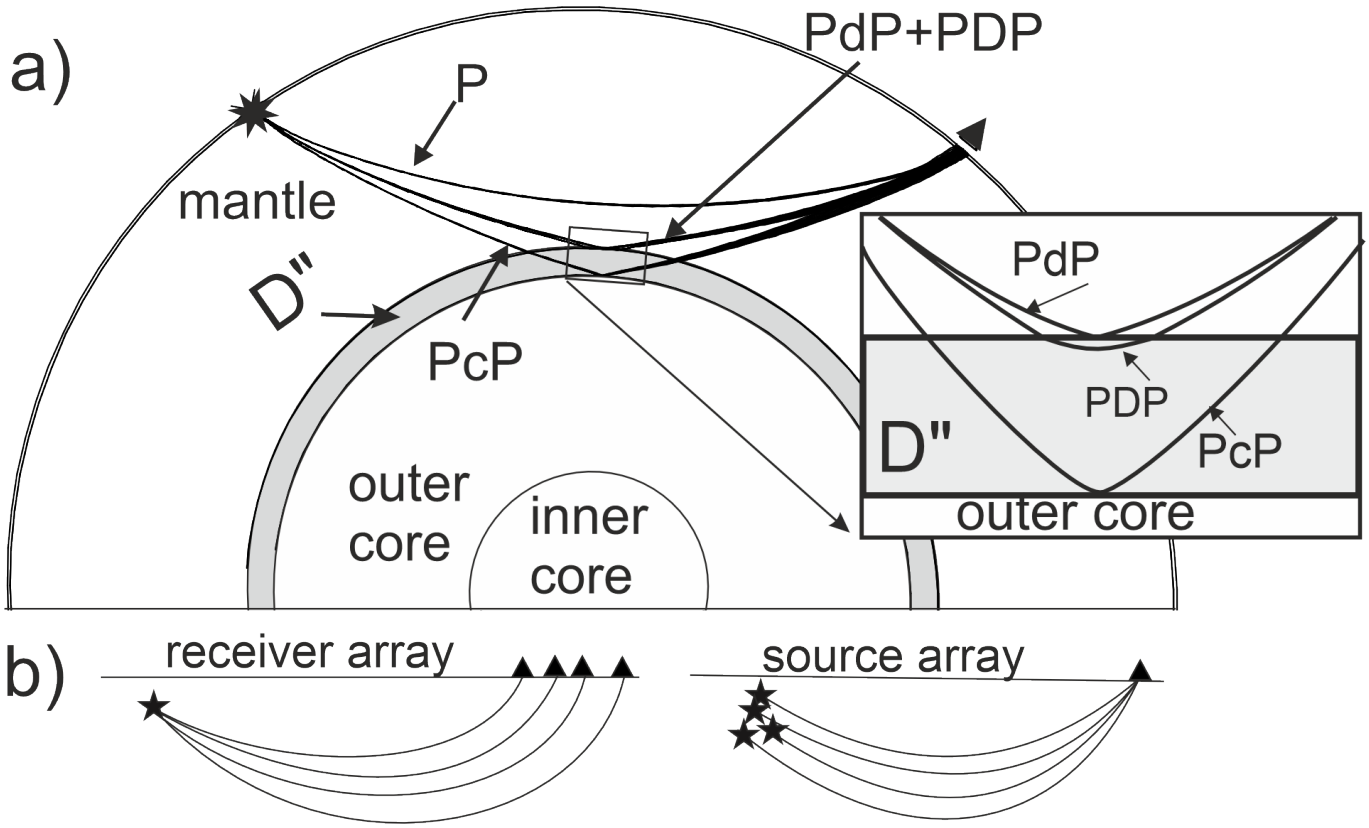

Figure 1 a) Cartoon showing the seismic waves used in our study (P, PcP and PdP). PdP, as it is used in the text, includes the reflection from the top of D", and the wave that travels through the layer (labelled PdP and PDP, as indicated in the inset), since at the distances used here, they cannot be separated as single arrivals. The star indicates an earthquake source, and the triangle denotes the receiver. Similar paths would be generated for S, SdS, and ScS. b) Schematic view of a receiver array and a source array.

and CASY in Antarctica. Figure 2 shows the locations of the stations we are using in this study, locations are also provided in Table S1.

Waveforms of events that occurred between 1990 and 2024 were acquired from the European Integrated Data Archive (EIDA) and Incorporated Research Institutions for Seismology (IRIS), which is now part of the EarthScope Consortium. The events have epicentral distances between 60 and 80 degrees to the stations DRV and RER, magnitudes between 5.5 and 7.0 and a depth range of 80 to 200 km. Further constraining the depth range, and using other depth intervals, resulted in too few traces (<7) to stack. The specified distance range is best for detecting P-wave reflections from the D" reflector (e.g., Weber, 1993; Cobden et al., 2015), and we focused on events with short, impulsive, high signal-to-noise ratio P-waves. Earthquakes with magnitude larger than 7 often have complicated, long-duration sources; hence, we restricted our magnitude range below this threshold.

34 events from the southern cluster (s.c., Fig. 2) met our criteria for the Indian Ocean stations, while the northern cluster (n.c. in Fig. 2) yielded 45 events for the Indian Ocean stations. However, after closer inspection between 11 and 15 events were kept for most of the Indian Ocean stations for the southern cluster, while only 2-5 events were usable from the northern cluster, which is too few events for a stack. The only exception is station MSEY, for which 21 events from the southern cluster and 9 events from the northern cluster could be used. For the Antarctic stations CASY, MAW and DRV we found 50 possible events from the northern and southern cluster. After closer inspection, only 27 (s.c.) and 9 events (n.c.) were retained for station DRV, 23 (n.c.) and 16 (s.c.) events for CASY, and 12 events from the southern cluster for MAW. The other events were dismissed because they either had noisy records or complicated source mechanisms. While there are potentially more stations available around the Indian Ocean, stations on Madagascar were too far from the sources, and the stations of the RHUM-RUM experiment and other stations on La Réunion and Mauritius did not yield enough events for stacking, which left us with the source-receiver combinations mentioned above. Similarly, the search for S-waves yielded very few events with clean, impulsive S-waveforms, and we therefore do not incorporate S-waves into the current analysis. Event parameters are shown in Table S2.

Figure 3 shows traces of the selected events for stations RER and CRZF. Both record sections include the same events, and clear differences in the waveforms can be seen. While the CRZF recordings have higher signal-to-noise ratios, those from RER show high-frequency signals superimposed on the longer-period signals visible for CRZF. Given this, it is necessary to filter the events. We tested 2nd order Butterworth bandpass filters of 0.3-3 s, 0.5-5 s, 1-10 s, 2-12 s and 3-25 s, and 5-50 s. While the source signals are fairly similar, they differ

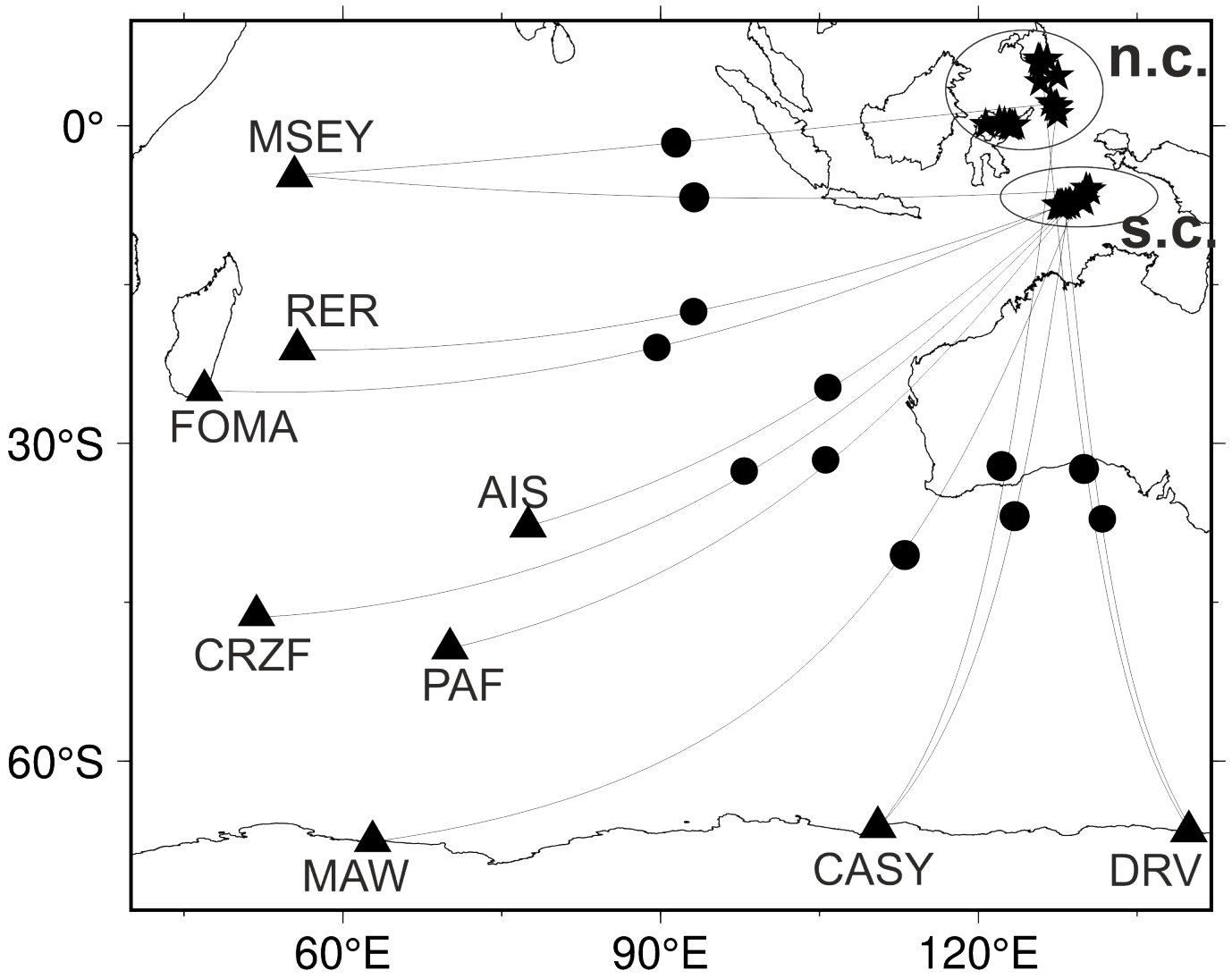

Figure 2 Receivers and sources. Stations are indicated by triangles, and earthquakes are denoted with stars and marked by s.c. for the southern cluster and n.c. for the northern cluster. Black circles show the reflection point of PdP for a model with a 300km thick D" region.

in the length and energy build-up within the waveform (i.e., the largest amplitude follows later in the source wavelet, e.g., 2012DEC10 or 2021DEC29 in Figure 3a and b). This may lead to artifacts in the analysis; therefore, we excluded some of these very complicated waveforms, as mentioned above. Example traces for stations FOMA, AIS, PAF, and DRV are shown in Figure S1. It is difficult to detect PdP waves in the single-trace seismograms, and even a PcP wave is difficult to distinguish, but this is common for P-waves at these distances, particular with noisy recordings.

3 Source Normalization Methods

A problem with stacking multiple events, especially when using natural earthquakes instead of nuclear tests, is their difference in focal mechanisms as mentioned above. While events in a given area often have similar source mechanisms, the emitted waveforms can differ significantly (compare Figures 3 and S1), and it is important to deconvolve the source before stacking in order to produce coherent D" reflections (e.g., Krüger et al., 1995, 1996; Reasoner and Revenaugh, 1999; Rost and Thomas, 2002). To overcome the problems associated with incoherent waveforms, we tested three different source-normalization methods: spiking deconvolution (SD), deconvolution with a Hilbert transform (HIL), and a cross-correlation (CORR) technique. Iterative deconvolution (ID, Ligorría and Ammon, 1999) was also considered, but did not produce reliable results. As a comparison, we also used events with similar direct P-waveforms without using a source normalization. We provide more details about each of the methods in the supplementary material.

Figure S2 shows examples of the original traces, the filtered but un-deconvolved traces (no normalization), and three source normalization methods (SD, CORR, and HIL) for events recorded by station PAF. As can be seen, each of the methods results in a different waveform. We find that the deconvolution window length (i.e., the time window used to identify the P-wavelet), impacts the obtained waveform as well as the coherence of the signals across the array. In addition, the deconvolution window length can cause a small time shift in the

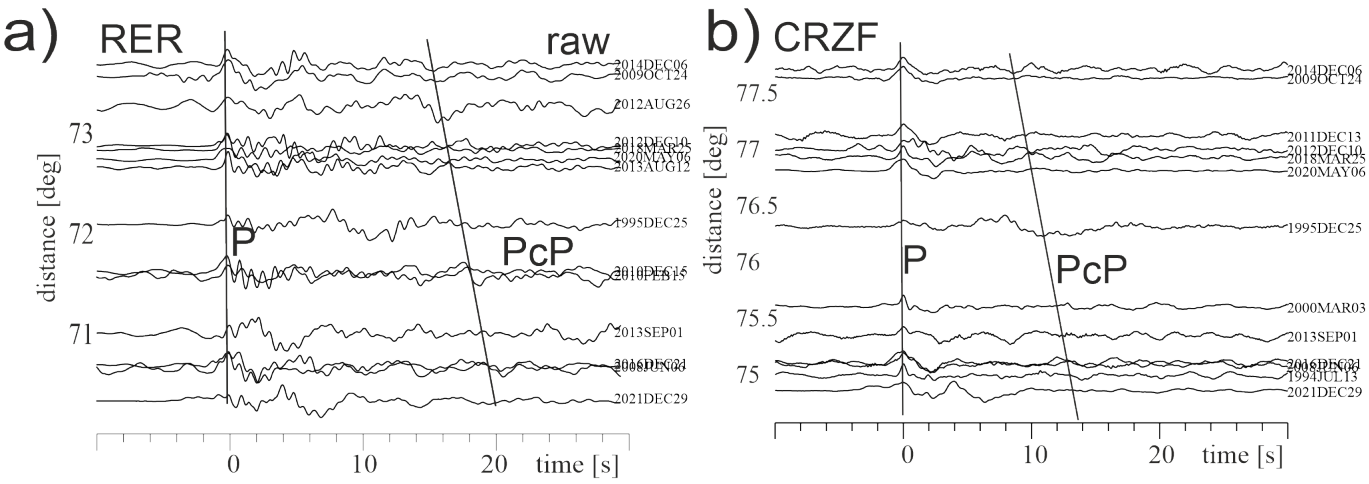

Figure 3 Distance-dependent seismogram sections of array events recorded at stations RER (a) and CRZF (b). The seismograms are neither filtered nor processed. Several events are the same for both source arrays. Traces are aligned on the P-wave arrival, and the theoretical arrival time for PcP is indicated, based on the distance and depth of the reference event (1995DEC25).

deconvolved trace relative to the original trace, depending on the chosen method and whether the deconvolution window starts before or at the actual P-wave onset. Unfortunately, in our data, the source-normalized traces still do not allow a clear PcP or PdP wave to be identified in single seismograms.

4 Source array vespagrams

Since the seismic traces both with and without source normalization do not show any clear reflections (Figures 3, S1, and S2), we use stacking methods to help improve the signal-to-noise ratio, thereby allowing us to identify arrivals by their slowness (Rost and Thomas, 2002). Small-amplitude P-wave arrivals, such as D" reflections, are not usually clearly visible in the time window between P and PcP in single traces given their small reflection coefficient (see also examples in Cobden et al., 2015; Jackson and Thomas, 2021). Furthermore, reported P-wave velocity contrasts are often smaller than S-wave velocity contrasts, based on observations of PdP and SdS and reflection coefficient modelling (e.g., Wysession et al., 1998; Cobden et al., 2015), making PdP signals more difficult to see than SdS.

For most array stacking techniques, the traces are shifted with relative time delays according to a plane wave arriving with slowness and backazimuth within a pre-determined range, and subsequently stacked (Schweitzer et al., 2009; Rost and Thomas, 2002). While this is straight forward for receiver arrays, when using source array, the depths of all earthquakes should be the same in order to calculate delay times for a plane wave. This, however, is usually not possible, either because the events are distributed over a relatively large depth range or because the error in their depths is up to several tens of kilometers. Therefore, originally, source arrays were designed to be used with sources for which location and depth of the explosions were known precisely (Krüger et al., 1995), which is the case for nuclear explosions but not for earthquakes. If the events have different depths, the relative travel-times for the P, PdP, and PcP phases will also vary in addition to travel-time variations from differences in distance.

Despite the known potential difficulties, we decided to test source vespagrams (e.g., Krüger et al., 1995), a fast and simple approach to stack traces after source normalization. The source-vespagram analysis is carried out using the calculated delay times for a range of slowness values, relative to the center event, and using the backazimuth of the central event (in the case of Figure 3, event 1995Dec25). In our study, we limit the depth range of the earthquakes from 80 to 200 km, and we filter the signals with lower frequencies (mostly below 0.5Hz) before applying the stacking techniques, hoping that small shifts in arrival time have due to event depths have a small influence on the stack.

Figure 4a shows the source vespagram for station CRZF, with a possible PdP marked. The Moho multiple (M) is enhanced in the source vespagrams, as described by Thomas et al. (2002), and it may be superimposed on the PcP or PdP arrivals, which may affect the stack (Lessing et al., 2015). The source vespagram for station FOMA (Figure 4b) shows a possible PcP arrival at a time expected for the CMB reflection, as well as the Moho multiple, but no clear PdP arrival is observed. This may possibly be due to the epicentral distances of the corresponding events (77-82 degrees), where P and PdP start to overlap. Figures 4c and 4d indicate a PdP arrival at station RER, whether source normalization was applied or not. As explained above and visible in Figure 4c and 4d, the source normalization changes the waveform. While the possible PdP phase is separate from other waves in panel 4d, the correlation removed part of the P-wave coda, making the Moho multiple more obvious. It should also be noted that PcP does not necessarily stack coherently in these vespagrams, likely due to time shifts between P and PcP given the different event depths, as explained above. As a test, we show a vespagram with initial alignment on the theoretical arrival times of PcP wave instead of the P-wave in Figure S3, where now the PcP wave is clearly visible,

but the P-wave arrival is less convincing.

Our results show that the different source depths still preclude the clear detection and picking of the PdP reflections in vespagrams. Consequently, slowness and time measurements taken from this analysis may be erroneous, and we do not rely on vespagram results. We carried out this exercise mainly to see whether a limited depth range and longer period signals would allow the detection of PdP waves, but find that our depth range is likely still too large.

5 Source array migration

Since the source vespagrams do not provide reliable PdP signals for D" interpretation, we extend our analysis to use a more complex seismic scattering imaging method, which is also called a simplified time migration (Thomas et al., 2004a,b). Therefore, this technique will be referred to as migration method throughout the remaining paper. Our aim here is to see whether the source-array migration method allows the detection of reflectors in the lowermost mantle, despite using events of different depth. The migration method does not rely on the plane-wave approximation (e.g., Thomas et al., 1999, 2004a), because the travel-times from a scatter point in the lowermost mantle (i.e., a point within a grid placed between 2400 and 2900 km depth, Figure 5) to the station (solid line in Figure 5) and to each event (dashed lines in Figure 5) are calculated separately using a 1D ray tracer and 1D velocity model ak135 (Kennett et al., 1995). These individually calculated travel times potentially make this approach more robust for source arrays. For each grid point, the traces are shifted with the calculated delay times relative to the center event and then stacked. The maximum amplitude in the time window (width of 3-5s) around the theoretical arrival time of the reflection for the center event is then measured and assigned to the respective scatter point in the grid. The large stacked amplitudes of a potential reflection will spread out along an isochrone, whose size decreases with increasing depth (i.e., when coming closer to the point of reflection, Figure S4). We pick the reflection depth (for either the D" reflection or the CMB reflection) where the large amplitude focuses (Figures 5, 6 and S5). The stacked amplitude at the theoretical reflection point is also displayed in an amplitude-depth profile (Figures 5, 6, 7, 8, S4, S5, S6 and S7), which further aids the identification of the reflections. More details about this method can also be found in Rost and Thomas (2002, 2009) as well as in Thomas et al. (1999, 2004a,b).

To verify that our approach produces reliable results, we generated synthetic data using the 1D reflectivity method (Müller, 1985), using a modified version of the ak135 velocity model that includes a 300 km thick D" region (based on model PWDK from Weber and Davis, 1990). The velocity contrast across the D" reflector was set to vary between 1% and 3%. Figure 6 shows an example for station PAF and a range of events with different depths (but all with a similar source wavelet, which allows to use the data without source normalization). Noise taken from real traces before the first P-wave arrival was added to the synthetics, and we chose the signal-to-noise ratio of the P-wave to be between 20 and 50%. As before, the signal traces and the source vespagram show only the P-wave as clear signal, but no PdP- or PcP-wave arrivals are visible (Figure 6 a, b). After applying the migration method (Figure 6c, d, e), the PdP arrival can still be resolved in the presence of noise, if the velocity contrast is larger than 1% (see also Kito et al., 2007).

The amplitude of the PdP wave in the amplitude-depth profile (Figure 6d) is reduced by the presence of noise, and also by the smaller velocity contrast. The test with synthetic data confirms that we can pick the PdP reflection despite noisy traces, and using events with different source depths. We also show that the thickness of the D" layer is recovered (within approx. 30 km). The example in Figure 6 also indicates that a velocity increase across the D" reflector (which we included in the 1D model in this example) generates a signal in the amplitude-depth profile, that has the same shape as PcP. This indicates that the polarity is the same as PcP, as we would expect. In the following, we also use this result to test the polarity of PdP waves in real data.

In the source-array migration, PcP sometimes focusses shallower in the mantle than at the CMB (Figure 7). This results from faster velocities within D" (Reasoner and Revenaugh, 1999), time shifts introduced by the source normalization, travel-time changes due to velocity variations in the mantle, and/or erroneous travel-time calculations caused by source location errors. Such time-shift variations would be visible as an apparent shift in the reflector depth within the migration results. Figure 7 shows the results of source-array migration using synthetic data and applying different source normalizations for station PAF. We tested different scenarios with D" velocity contrasts between -3% and +3%, which covers the range of suggested P- and S-wave velocity contrasts from previous studies (Wysession et al., 1998; Cobden et al., 2015), although we note that 3% contrasts are more common for S-waves than for P-waves. While a large P-wave velocity contrast in our study is unlikely, such contrasts may vary laterally and hence may affect the observed time-shifts relative to the reference model. In our synthetic data (Figures 6 and 7), we do observe shifts in apparent reflector depths (by up to 20-30 km), but the D" thickness of 300 km is still recovered in Figures 6 and 7, since PcP also shifts by a similar amount. However, possible velocity variations within the D" layer may cause variations in the PcP arrival times, and therefore lead to an apparent thickness change of the D" layer. Based on our synthetic tests, we assign an average error of 30 km to the recovered thickness of the D" layer. In addition, we note that the source normalization does not change the polarity of the D" reflection relative to the direct P-wave.

Based on these tests, we do not use the depth of the reflector directly as determined by the migration method, but instead we use the amplitude-depth profiles to measure the thickness of the D" layer. We note that we did not apply a tomography correction since earthquake depths often have errors of several kilometers and are therefore already contributing to any time shifts in the data. Also, as detailed by Koroni and Trampert (2015),

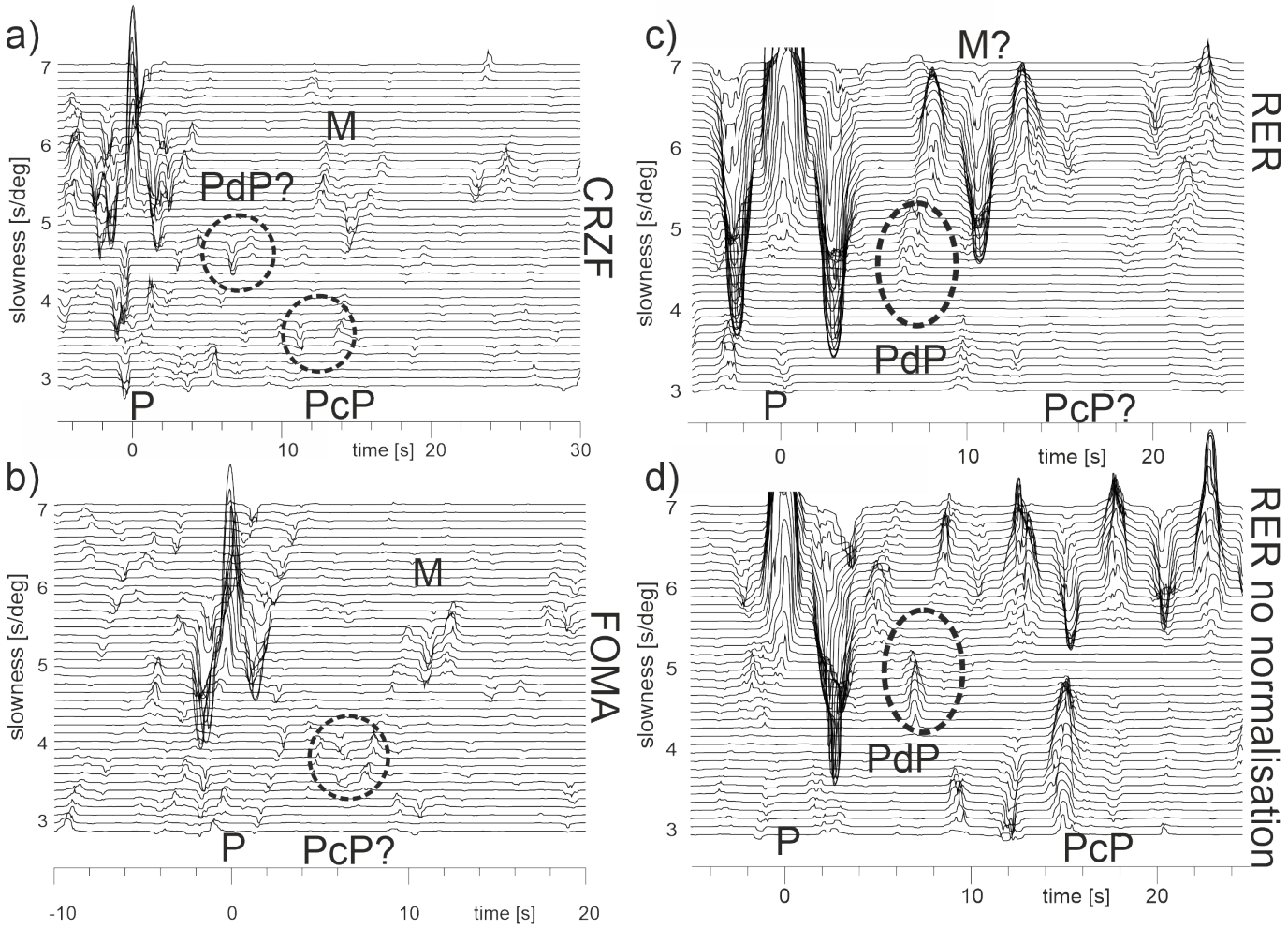

Figure 4 Source-array vespagrams for stations a) CRZF (central epicentral distance: 76 degrees), b) FOMA (central epicentral distance: 79.5 degrees), and c)-d) RER (central epicentral distance: 72 degrees). All vespagrams are aligned on the P-wave arrivals; PcP and a possible PdP are marked by dashed ellipses. In panels a) and b), a Butterworth bandpass filter of 0.5 to 5 s has been applied, while in panels c) and d), a Butterworth filter of 3 to 25 s has been used. Panels a) - c) were all source normalized with the CORR method, but no normalization was applied in panel d). The arrival at ~10s after the P-wave in panels a) - c) is likely the Moho multiple (M), which is enhanced in the source stack. Note that it is not clear whether PdP is present in panel b), likely due to the large event distances, which may cause superposition of the P and PdP waves.

travel-time corrections based on tomographic models can introduce additional errors, and P-wave tomography models for this region are quite variable (e.g., tomography models provided in Submachine, Hosseini et al., 2018, see also Figure S6). Our synthetic test also confirm that velocity variations in the mantle, without a D" reflector, do not generate arrivals between P and PcP (Figure S7).

After analyzing source-array migrations for the Indian Ocean stations, we found that station AIS could not be used since, unfortunately, the events recorded at this station fell into two separate clusters, 10 degrees apart from one another. There were too few events per cluster (Figure S1), which resulted in very noisy stacks with low slowness resolution. For station FOMA (Figure S1) and other stations on Madagascar, the events have long epicentral distances (~80 deg), so the P and PcP arrivals were very close together as shown on the corresponding vespagrams (Figure 4). The migration could not separate the arrivals; therefore, we had to exclude this station as well. Source stack and migration results for nearby station RER are shown in Figures 4c, 4d, and 5, and they indicate a weak reflector with a velocity increase at ~250 km above the CMB. Further south, station CRZF shows a reflector at ~270 km above the CMB (Figure S5a) with very small amplitude in the amplitude-depth profile, while the result for station PAF indicates a possible PdP signal consistent with a reflector 220 km above the CMB (Figure S5b). The polarities of PdP waves for those two stations are the same as for PcP, and therefore would indicate a velocity increase across D". The scatter images from the migration for station PAF are not as clear as for station RER, but the synthetic example in Figure 6 shows that stacked amplitudes in the amplitude-depth profile are expected to be small for PAF, due to the short epicentral distance of around 63 degrees. Furthermore, possible reflections differed between the source normalization results for PAF and the PcP wave is not clearly identified in the amplitude-depth profiles. We are therefore cautious with the interpretation of a potential reflectors for stations PAF and CRZF. Station MSEY located in the Seychelles (Figure S6b) im-

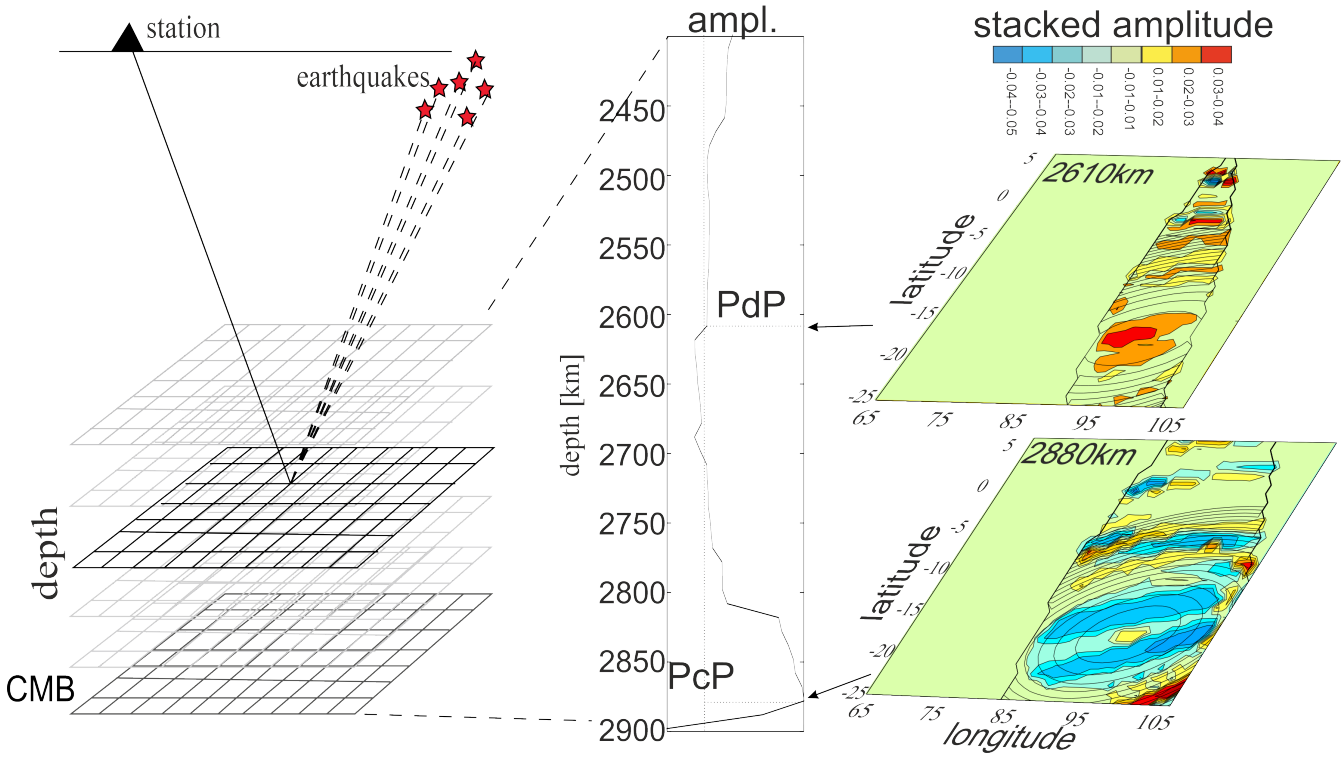

Figure 5 Cartoon illustrating the applied migration technique (left panel), together with an amplitude-depth profile (middle panel) and stacked amplitudes for two depths for station RER with source normalization CORR applied (right panel). The seismic traces of RER were filtered with a Butterworth bandpass filter from 3 to 25s. Ray paths from each earthquake to the grid are shown by dashed lines, and the ray paths from the grid point to the station is indicated by the solid line. For each layer, the maximum amplitude at the theoretical reflection point for the central event is used to construct the amplitude-depth profiles (middle panel). Two depth layers (2610 and 2860 km) showing the corresponding amplitude distribution at each grid point, determined at the arrival time for a predicted reflection (right panel).

ages the lowermost mantle further north than our other source array-event combinations and for this station we found a thickness of 200 km for the D" layer.

In addition to the Indian Ocean stations, we also examined stations MAW, CASY and DRV in Antarctica (Figures 8, S6). Station DRV had the largest number of available events from both clusters, resulting in better noise suppression and cleaner stacks especially for the southern cluster, but the distribution of the events (Figure S1) is not well suited to resolve the slowness of different seismic phases in the vespagram (the large amplitudes are spread over a larger slowness range) even though it still allows us to detect arrivals (Figure 8, top). We did identify an arrival in the source vespagram at a time consistent with a reflector close to the CMB which is in agreement with the amplitude-depth profile that indicates a D" reflector 190 km above the CMB. The polarity of the PdP wave is the same as PcP and therefore indicates a velocity increase across D". Amplitude depth profiles for CASY and MAW are shown in Figure S6 and confirm the results from DRV with the presence of a reflector between 160 and 230 km above the CMB.

6 Discussion

For investigating the D" region beneath the Indian Ocean, we used source arrays and tested several source normalization methods prior to stacking. Previous work has usually relied only on the SD technique. Based on our synthetic tests, we mostly relied on CORR results, but we tried to confirm our findings with other source normalizations, too, thereby helping us to decide whether a signal in the source-array stack was a processing artifact or a real feature.

Despite using different source normalizations, we were not able to detect clear PdP- or PcP waves in the source vespagrams, likely due to the different event depths. Even limiting the focal depth range and focusing on longer periods (greater than 2 s) did not provide reliable results, but other regions that have more events in an even smaller depth range could prove more suitable. The double-array stacking techniques (or double-beam methods) employed in previous D" studies (e.g., Kito et al., 2004; Lay et al., 2004; Hutko et al., 2009; Scherbaum et al., 1997; Yamada and Nakanishi, 1996, 1998) are likely more powerful than those only based on source arrays since the combined source- and receiver-arrays allow for better noise suppression and clearer D" reflections. It would be useful to compare our source arrays to receiver stacks or combine source arrays and receiver arrays (e.g., Kito et al., 2004) to further examine the lower mantle beneath the Indian Ocean, but the data availability is limited at the moment. OBS data from the RHUM-RUM experiment near La Réunion (Barruol and

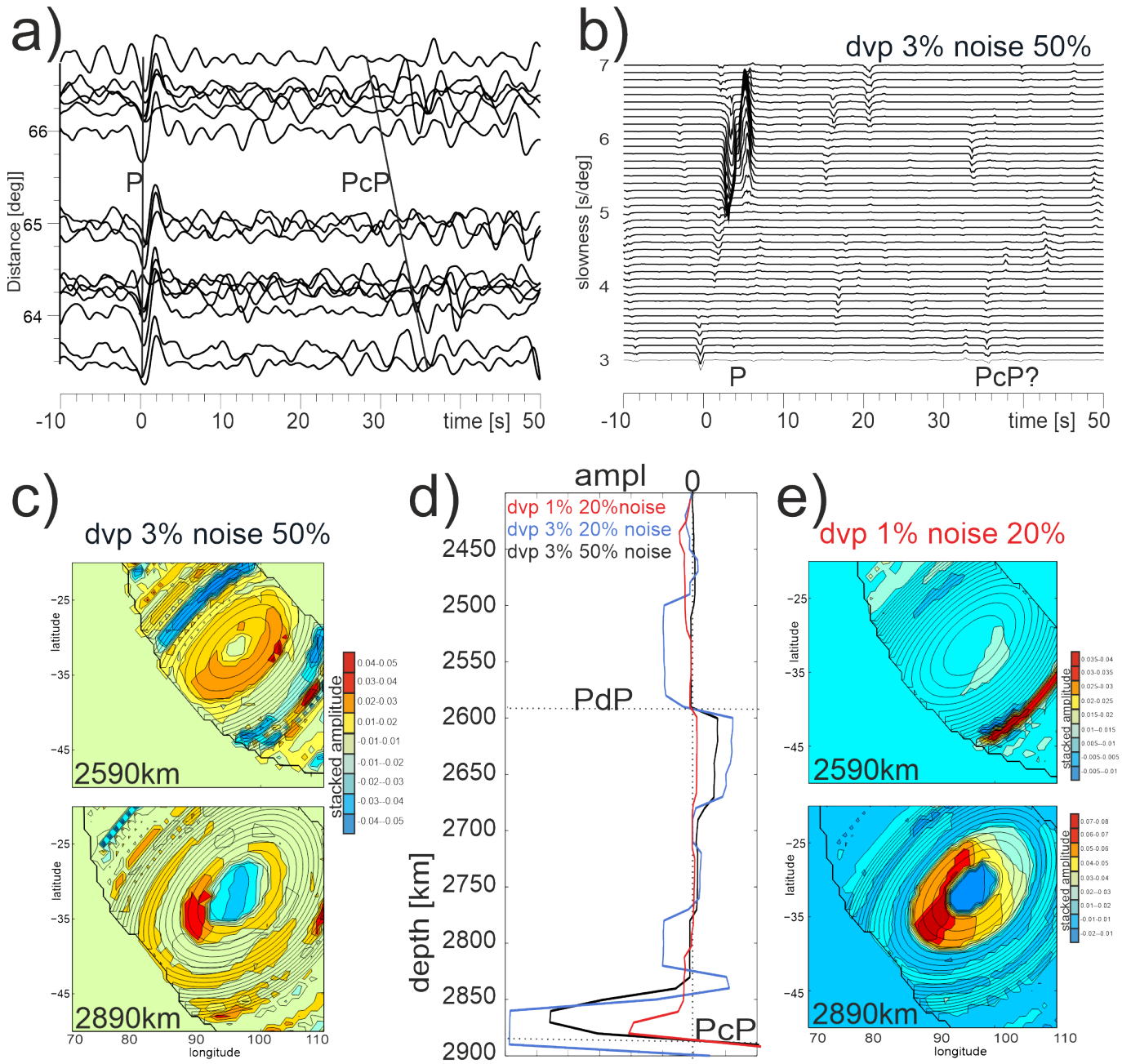

Figure 6 a) Synthetic seismic traces calculated for a dominant period of 3s for 15 events, using a modified ak135 model with D" reflector (dvp +3%), 300km above the CMB. We used distances corresponding to the events recorded by station PAF. Real noise, taken from recordings without earthquake signal, and scaled to 50% of the P-amplitude has been added to the traces. Traces are aligned on the P-wave arrival, and the predicted arrival of the PcP-wave for the center event is indicated. b) Source-array vespagram as in Figure 4 for the traces in a). The predicted arrival times of the P- and PcP-wave are indicated. c) Migration (as in Figure 5) for the traces in a), showing the focusing of energy of the PdP arrival (top) and the PcP arrival (bottom) with respective depths. Color scale denotes amplitude. d) Amplitude-depth profiles for three migrations, with the red line showing the results for dvp +1%, 20% noise, the blue line shows the result for dvp +3%, 20% noise, and the black line gives the result for dvp +3%, 50% noise (corresponding to panel c)). The depth for PdP and PcP are indicated by the dashed line. e) Same as in panel c) but for dvp 1% and 20% noise (corresponding to the red line in panel d)).

Sigloch, 2013) are deployed in a similar region as the GEOSCOPE stations we used; however, the number and the data quality of events recorded by these OBS stations was not sufficient to use them as receiver array or in double-array (or double-beam) stacks. We could, however, find four suitable source-receiver combinations, using arrays at the eastern African coast and Madagascar and an array in Australia, but found only events that reflect further north than the RER reflection point, i.e., in a similar region, where Young and Lay (1987) find a D" layer with a thickness of 280 km. The two events in Figure S8 show PdP arrivals as well as SdS arrivals, with a thickness of D" in this region of 280-290 km, in agreement with Young and Lay (1987). A reverse path (Indian Ocean events to Australia) provided a thickness measurement of around 300 to 320 km for the D" layer. Our velocity contrast is, however, likely smaller than 2.8%, since the amplitudes of PdP in all these cases are

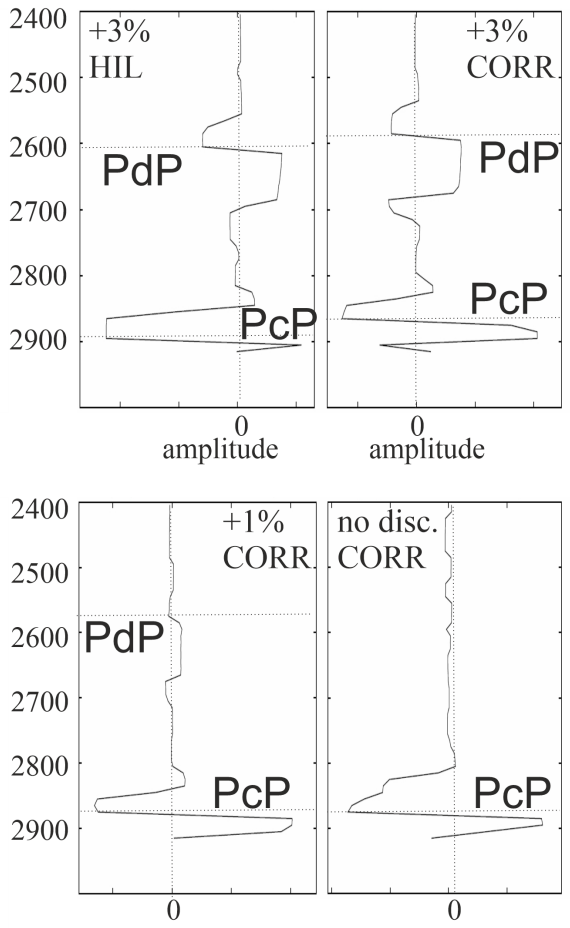

Figure 7 Results from source-array migration using synthetic data with dominant period of 3s for station PAF. The D" velocity variations and the applied source-normalization approach are indicated in each panel, and the depths of imaged reflectors are indicated by dashed lines. The lower dashed line indicates the depth of the PcP reflection. Small shifts in estimated reflector depths are caused by the deconvolution process and the chosen deconvolution window length for the P-wavelet.

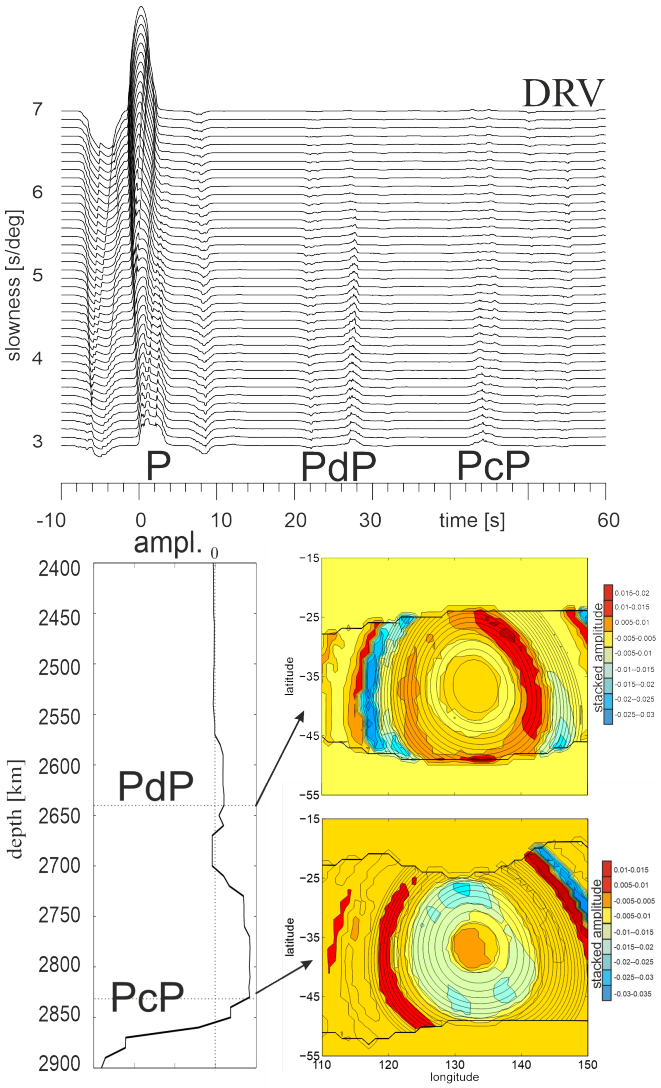

Figure 8 Source vespagram (top panel) and amplitude-depth profile (bottom left panel) from the migration for station DRV (filter 10-50 s, CORR). The P, PdP, and PcP waves are indicated in the vespagram, and the PdP and PcP depths from the migration are indicated by dashed lines in the amplitude-depth profile. The bottom right panel shows the amplitude distributions for PcP and PdP as in Figure 5.

smaller than expected for an almost 3% velocity contrast (see e.g., Cobden et al., 2015).

The migration method we used here provides more reliable results for lowermost mantle reflectors for source arrays since it does not rely on the assumption of a plane wave. Source-array stacks (Krüger et al., 1995, 1996) and double-array stacks created with a technique similar to our migration method have been applied to investigate the D" reflector in previous studies (Kito and Krüger, 2001; Kito et al., 2004; Scherbaum et al., 1997). The large number of sources and receivers used in these investigations sometimes even permitted more than one discontinuity in the D" layer (or perhaps even large-scale scatterers) to be detected.

Our results for the D" reflections are summarized in Figure 9, superimposed on the vote map (Shephard et al., 2017) for high-velocities in P-wave tomographic models (as provided in Submachine, Hosseini et al., 2018) for a depth of 2600 km, as the D" reflector has been associated with subducted lithosphere in the past (e.g., Lay, 2015). The reflection points for PAF and CRZF are inferred to be located in an average-velocity portion of the lowermost mantle, while only the reflection points for station MSEY, RER, CASY, MAW and DRV are within a high-velocity area. We note, however, that tomographic models for this region differ significantly as suggested by the low number of models agreeing on high velocities in the vote maps in Figure 9 (in contrast to the low velocities further west, as shown in Figure S9 that are likely due to the LLSVP beneath Africa).

We mark the deep slab near Indonesia (Simmons et al., 2015), in the region where our reflection points are located (S+15 in Figure 9). The imaged high-velocity region in the Simmons et al. (2015) model is shown at 2371 km depth, but we note in their work that this high velocity anomaly also extends to deeper depths and lat-

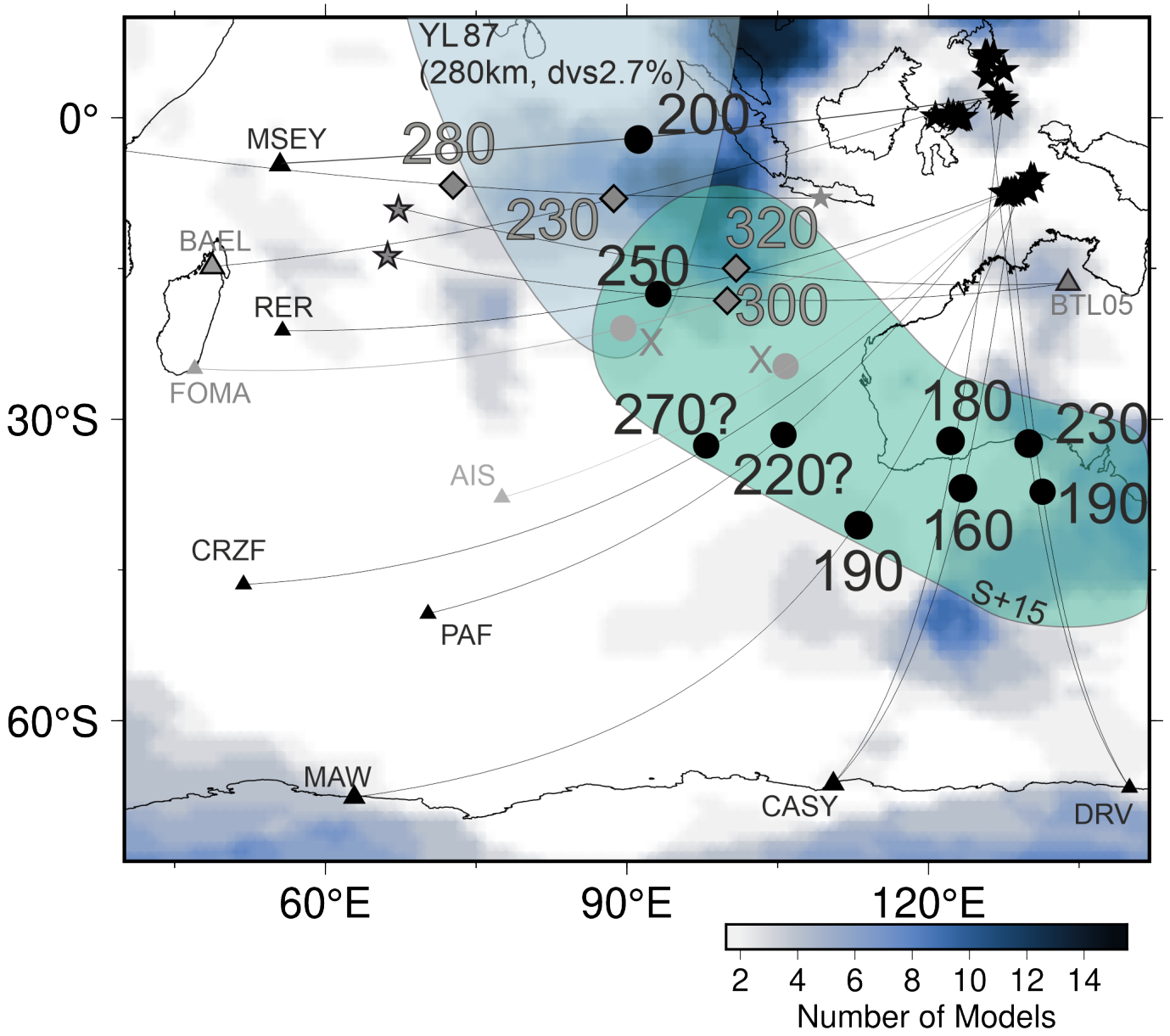

Figure 9 Map of D" reflection locations. Sources are denoted by stars, and receivers are denoted by triangles. The thickness of the reflector was estimated for several stations (black triangles) and are given next to each reflection point. As discussed in the text, the reflector for station PAF and CRZF have higher uncertainty. The stations marked by grey triangles were either too far (FOMA), or had too few traces to generate a robust stack (AIS). We also show with grey diamonds two reflection point in the north, where receiver arrays in Madagascar (grey triangle with black outline) and Ethiopia show a reflection in P and S-waves (Fig S6, Table S3). A reverse path (grey stars with black outline in the Indian Ocean to an array in Australia (grey triangle with black outline) and their thickness estimate are also given. The region where Young and Lay (1987) imaged D" with S-waves is shown by the blue-grey shaded area labelled YL87, and their estimated depth and S-velocity contrast are also listed. The location of the subducted slab at 2371 km depth indicated by Simmons et al. (2015) is shown by the green shaded area, labelled S+15. The underlying vote map for high-velocities is generated for the depth of 2600 km, and using P-wave tomography models provided in Submachine (Hosseini et al., 2018). For comparison, the vote map for low velocities is shown in Figure S9.

erally covers a portion of the CMB. Since several of our reflection points are found within this high velocity region, we suggest that our imaged reflections are detecting the top of this subducted lithosphere. Our amplitude-depth profiles suggest a small signal for PdP with a polarity that is the same as that for the PcP (Figures 5, 8, and S5), which indicates the presence of a small velocity increase across the reflector, further agreeing with the interpretation of the reflections resulting from a remnant piece of cold subducted lithosphere. The polarities of PdP in Figures 5 and 8 and their interpretation of faster than average material in D" can also explain the travel-times for the CMB reflection, which focus PcP in the migration above the CMB. The inferred positive velocity contrast, however, suggests that MgSiO3 ppv is likely not present in this area since it would be associated with a negative P-wave velocity contrast (Wookey et al., 2005; Cobden et al., 2015,

Thomas et al. 2022). That said, alignment of ppv mineral grains (i.e., anisotropy) could lead to different results (Pisconti et al., 2019, 2022) and still permit for post-perovskite to be present.

Our results for station RER agree with results by Young and Lay (1987) (indicated in Figure 9 as YL87). While the mapped region of YL87 only extends to the reflection point of RER, several of our other stations provide D" discontinuity detections further to the south, indicating that the structure at the top of the D" region continues. Results for MSEY show a slightly thinner D" layer (190-200km with error of 30km) further north than RER while our receiver array results again agree with those of YL87. West of our reflection points, Wright and Kuo (2007) found evidence for a discontinuity around 210 km above the CMB and Kendall and Shearer (1994, 1995) investigated a similar region with S-waves as used in our study and found inconclusive evidence for a D" reflector in their small number of source-receiver combinations. In addition, Weber and Körnig (1992) used ISC data to investigate the deep mantle structure in this region, but found only low-quality, inconclusive results. The small velocity jump found by Wright and Kuo (2007) agrees with the small amplitudes of PdP waves in our amplitude depth profiles. Since the results by YL87 show a much stronger S-wave contrast of 2.7% this could either mean that the velocity contrast decreases towards the south and west or that the P-wave contrast is much smaller than the S-wave contrast.

The estimated D" thickness seems to decrease to the south, indicating a thinning of the subducted lithosphere, if reflections are indeed due to mapping the top of a subducted slab. Considering the results of Wright and Kuo (2007) the thickness decreases also to the West of our reflection points. To further evaluate this structure, it would be instructive to examine crossing ray paths that could confirm the D" reflections and test for D" anisotropy (e.g., Pisconti et al., 2022), but we could not find a sufficient number of source-receiver combinations crossing the Indian Ocean in different directions to facilitate such a study. In a compilation of anisotropy in the lowermost mantle, Wolf et al. (2023) also show little evidence for D" anisotropy beneath the Indian Ocean with some studies showing inconclusive or no anisotropy (Creasy et al., 2017; Rao et al., 2017). On the other hand, near our reflection points for stations DRV, MAW, and CASY, Usui et al. (2008) find evidence for anisotropy in S-waves. Their SH-velocity model has a discontinuity with velocity increase at 2550 km depth, while their SV-velocity profile has a positive gradient to the CMB, starting at 2741 km depth. Our P-wave results suggest a discontinuity 160-230 km above the CMB. Analyses of source arrays using S-waves could also help to further establish the source of the D" reflector in the region of the Indian Ocean; however, our data were not of high enough quality to collect a sufficient number of S-wave traces.

Understanding the structures, and therefore the mineralogy, at the CMB could also help us to understand how lowermost mantle velocity anomalies influence core convection, as suggested for the high-latitude magnetic flux patches beneath Siberia and Canada (e.g., Gubbins et al., 2007). In these areas, the lowermost mantle seems to be associated with an anomalous thermal boundary above the outer core that could influence core flow. Away from the high latitude regions, the geomagnetic field map gufm1 (Jackson et al., 2000) shows high magnetic flux patches that move from the southern hemisphere northwards to the west of Indonesia, before changing direction and moving westwards in the time-frame of several centuries. Since the region where this change in direction occurs is close to our study region, the likely colder, deep subducted slab imaged by our reflection points and by Simmons et al. (2015) could affect the core convection in a similar way to the results by Gubbins et al. (2007).

Finally, since the source-array migration method only requires one seismometer, it could be suitable for seismology on other planets, such as Mars. Recently, Stähler et al. (2021) detected a reflection in the seismic recordings of the InSight seismometer, which they interpreted as a core-reflected ScS wave. The migration method relies on knowing the velocities inside the planet, but after constraining the velocity structure of the Martian mantle, a source stack or source-array migration could further help to constrain or confirm the depth of the Martian core.

7 Conclusion

In this study, our aim was to test whether source arrays, and particularly a source-array migration method, can be used to study the D" region, by applying the method to the previously sparsely sampled D" reflector beneath the Indian Ocean. Since there are very few land stations at appropriate epicentral distances and only one OBS experiment available to generate receiver-array or double-array stacks, we used source arrays and stacked events that are in a relatively narrow depth range (80-200 km) for each of the stations, assuming that a limited depth range would provide more reliable source stacks. However, we found that our depth range was likely still too large for source-array vespagrams. Noise in the data and the plane-wave approximations also limit the resolution of source-array stacks. Source-array migration works better and is a useful method that circumvents the plane-wave assumption for calculating delay times between traces that was required for the vespagram analysis. Given the different event depths, the ability to calculate individual travel-times for each point within a lower mantle grid leads to more robust results. Even though the reflections are weak in some cases, our results suggest a D" layer thickness south of Australia of 160-230 km, whereas beneath the central Indian Ocean, north and west of Australia, we find a thicker D" layer whose upper boundary is at 250-270 km and up to 320 km using a receiver array and agreeing with previously mapped D" thickness. While tomographic models show a range of velocity variations beneath the Indian Ocean, our D" reflection points agree with ancient subducted lithosphere in this region (Simmons et al., 2015).

Our results show that source-array migration allows to image the D" reflector, despite a low number of events per station. Future work, using other event locations

and focal depth ranges, could help us to gain a more complete picture. In addition, a source-depth relocation (Florez and Prieto, 2017) prior to the migration could help to improve the results. It was useful to investigate the effects of source normalization on the traveltimes, since signal detections in the stacks could be verified by using multiple source-normalization methods. In addition, the source-array migration results could also be tested against receiver-array migration result, if suitable arrays become available. These may contribute crossing ray paths that would allow anisotropy in D" to be constrained (e.g., Thomas et al., 2011; Pisconti et al., 2019, 2022).

Acknowledgements

We would like to thank four anonymous reviewers, L. Waszek and R. Anthony for comments on this and a previous version of this manuscript. This work was partly supported by the Norwegian Research Council through its Centres of Excellence scheme, project numbers 223272 (CEED) and 332523 (PHAB), the Young Research Talents project 326238 (POLARIS), and DFG grant TH1530/25-1 (as part of the SPP 2404: DeepDyn). Maps were produced with GMT (Wessel and Smith, 1995), and seismic data were analyzed with Seismic Handler (Stammler, 1993).

Data and code availability

Seismograms from the GEOSCOPE stations (FDSN network G) used in this study were obtained from EIDA using the IPGP Data Center (www.ipgp.fr), RESIF (ws.resif.fr), and IRIS (www.iris.edu) (last accessed May 2023). Information on the GEOSCOPE network can be found in: Institut de physique du globe de Paris (IPGP) and École et Observatoire des Sciences de la Terre de Strasbourg (EOST) (1982). Seismic Handler is freely available (http://www.seismic-handler.org), and all required codes for the source migration and the vespagram analysis are available on Zenodo (Heyn and Thomas, 2025, doi: 10.5281/ZENODO.15426460).

Tables outlining station locations and DOI for each station/array as well as events used in this study are provided in the supplemental material.

Competing interests

The authors have no competing interests.

References

Barruol, G. and Sigloch, K. Investigating La Réunion Hot Spot From Crust to Core. *Eos, Transactions American Geophysical Union*, 94 (23):205–207, June 2013. doi: 10.1002/2013eo230002.

Bullen, K. E. An earth model based on a compressibility pressure hypothesis. *Geophysical Journal International*, 6:50–59, Mar. 1950. doi: 10.1111/j.1365-246x.1950.tb02973.x.

Cobden, L., Thomas, C., and Trampert, J. *Seismic Detection of Post-perovskite Inside the Earth*, page 391–440. Springer International Publishing, 2015. doi: 10.1007/978-3-319-15627-9_13.

Creasy, N., Long, M. D., and Ford, H. A. Deformation in the lowermost mantle beneath Australia from observations and models of seismic anisotropy. *Journal of Geophysical Research: Solid Earth*, 122(7):5243–5267, July 2017. doi: 10.1002/2016jb013901.

Douet, V., Vallée, M., Zigone, D., Bonaimé, S., Stutzmann, E., Maggi, A., Pardo, C., Bernard, A., Leroy, N., Pesqueira, F., Lévêque, J.-J., Thoré, J.-Y., Berc, M., and Sayadi, J. The GEOSCOPE broadband seismic observatory. *EGU General Assembly*, 18:2016–8867, 2016.

Florez, M. A. and Prieto, G. A. Precise relative earthquake depth determination using array processing techniques. *Journal of Geophysical Research: Solid Earth*, 122(6):4559–4571, June 2017. doi: 10.1002/2017jb014132.

Garnero, E. J., McNamara, A. K., and Shim, S.-H. Continent-sized anomalous zones with low seismic velocity at the base of Earth's mantle. *Nature Geoscience*, 9(7):481–489, June 2016. doi: 10.1038/ngeo2733.

Greff-Lefftz, M., Métivier, L., Panet, I., Caron, L., Pajot-Métivier, G., and Bouman, J. Joint analysis of GOCE gravity gradients data of gravitational potential and of gravity with seismological and geodynamic observations to infer mantle properties. *Geophysical Journal International*, 205(1):257–283, Feb. 2016. doi: 10.1093/gji/ggw002.

Gubbins, D., Willis, A. P., and Sreenivasan, B. Correlation of Earth's magnetic field with lower mantle thermal and seismic structure. *Physics of the Earth and Planetary Interiors*, 162(3–4):256–260, July 2007. doi: 10.1016/j.pepi.2007.04.014.

Haddon, R. and Cleary, J. Evidence for scattering of seismic PKP waves near the mantle-core boundary. *Physics of the Earth and Planetary Interiors*, 8(3):211–234, May 1974. doi: 10.1016/0031-9201(74)90088-0.

Hedlin, M. A. H. and Shearer, P. M. An analysis of large-scale variations in small-scale mantle heterogeneity using Global Seismographic Network recordings of precursors to PKP. *Journal of Geophysical Research: Solid Earth*, 105(B6):13655–13673, June 2000. doi: 10.1029/2000jb900019.

Heyn, B. and Thomas, C. Investigating the D" Reflector Beneath the Indian Ocean with Source Arrays, 2025. doi: 10.5281/ZENODO.15426460.

Hosseini, K., Matthews, K. J., Sigloch, K., Shephard, G. E., Domeier, M., and Tsekhmistrenko, M. SubMachine: Web-Based Tools for Exploring Seismic Tomography and Other Models of Earth's Deep Interior. *Geochemistry, Geophysics, Geosystems*, 19(5): 1464–1483, May 2018. doi: 10.1029/2018gc007431.

Hutko, A. R., Lay, T., and Revenaugh, J. Localized double-array stacking analysis of PcP: D" and ULVZ structure beneath the Cocos plate, Mexico, central Pacific, and north Pacific. *Physics of the Earth and Planetary Interiors*, 173(1–2):60–74, Mar. 2009. doi: 10.1016/j.pepi.2008.11.003.

Institut de physique du globe de Paris (IPGP) and École et Observatoire des Sciences de la Terre de Strasbourg (EOST). GEOSCOPE, French Global Network of broad band seismic stations, 1982. doi: 10.18715/GEOSCOPE.G.

Jackson, A., Jonkers, A. R. T., and Walker, M. R. Four centuries of geomagnetic secular variation from historical records. *Philosophical Transactions of the Royal Society of London. Series A: Mathematical, Physical and Engineering Sciences*, 358(1768):957–990, Mar. 2000. doi: 10.1098/rsta.2000.0569.

Jackson, J. M. and Thomas, C. Seismic and Mineral Physics Constraints on the D" Layer, June 2021. doi: 10.1002/9781119528609.ch8.

Kendall, J. and Shearer, P. M. Lateral variations in D" thickness from long-period shear wave data. *Journal of Geophysical Research: Solid Earth*, 99(B6):11575–11590, June 1994. doi:

10.1029/94jb00236.

Kendall, J.-M. and Shearer, P. On the structure of the lowermost mantle beneath the southwest Pacific, southeast Asia and Australasia. *Physics of the Earth and Planetary Interiors*, 92(1–2): 85–98, Nov. 1995. doi: 10.1016/0031-9201(95)03063-3.

Kennett, B. L. N., Engdahl, E. R., and Buland, R. Constraints on seismic velocities in the Earth from traveltimes. *Geophysical Journal International*, 122(1):108–124, July 1995. doi: 10.1111/j.1365-246x.1995.tb03540.x.

Kito, T. and Krüger, F. Heterogeneities in D" beneath the southwestern Pacific inferred from scattered and reflected P-waves. *Geophysical Research Letters*, 28(13):2545–2548, July 2001. doi: 10.1029/2000gl012801.

Kito, T., Krüger, F., and Negishi, H. Seismic heterogeneous structure in the lowermost mantle beneath the southwestern Pacific. *Journal of Geophysical Research: Solid Earth*, 109(B9), Sept. 2004. doi: 10.1029/2003jb002677.

Kito, T., Rost, S., Thomas, C., and Garnero, E. J. New insights into the P-and S-wave velocity structure of the D'' discontinuity beneath the Cocos plate. *Geophysical Journal International*, 169 (2):631–645, May 2007. doi: 10.1111/j.1365-246x.2007.03350.x.

Koelemeijer, P. Toward Consistent Seismological Models of the Core–Mantle Boundary Landscape, June 2021. doi: 10.1002/9781119528609.ch9.

Koroni, M. and Trampert, J. The effect of topography of upper mantle discontinuities on SS precursors. *Geophysical Journal International*, 204(1):667–681, Dec. 2015. doi: 10.1093/gji/ggv471.

Krüger, F., Weber, M., Scherbaum, F., and Schlittenhardt, J. Evidence for normal and inhomogeneous lowermost mantle and core-mantle boundary structure under the Arctic and northern Canada. *Geophysical Journal International*, 122(2):637–657, Sept. 1995. doi: 10.1111/j.1365-246x.1995.tb07017.x.

Krüger, F., Scherbaum, F., Weber, M., and Schlittenhardt, J. Analysis of asymmetric multipathing with a generalization of the double-beam method. *Bulletin of the Seismological Society of America*, 86(3):737–749, June 1996. doi: 10.1785/bssa0860030737.

Lay, T. *Deep Earth Structure: Lower Mantle and D"*, page 683–723. Elsevier, 2015. doi: 10.1016/b978-0-444-53802-4.00019-1.

Lay, T. and Helmberger, D. V. A lower mantle S-wave triplication and the shear velocity structure of D". *Geophysical Journal International*, 75(3):799–837, Dec. 1983. doi: 10.1111/j.1365-246x.1983.tb05010.x.

Lay, T., Berger, J., Buland, R., Butler, R., Ekström, G., Hutt, C., and Romanowicz, B. *Global Seismic Network Design Goals Update 2002*. IRIS, Washington, D.C, 2002.

Lay, T., Garnero, E. J., and Russell, S. A. Lateral variation of the D" discontinuity beneath the Cocos Plate. *Geophysical Research Letters*, 31(15), Aug. 2004. doi: 10.1029/2004gl020300.

Lessing, S., Thomas, C., Saki, M., Schmerr, N., and Vanacore, E. On the difficulties of detecting PP precursors. *Geophysical Journal International*, 201(3):1666–1681, Apr. 2015. doi: 10.1093/gji/ggv105.

Ligorría, J. P. and Ammon, C. J. Iterative deconvolution and receiver-function estimation. *Bulletin of the Seismological Society of America*, 89(5):1395–1400, Oct. 1999. doi: 10.1785/bssa0890051395.

Mancinelli, N., Shearer, P., and Thomas, C. On the frequency dependence and spatial coherence of PKP precursor amplitudes. *Journal of Geophysical Research: Solid Earth*, 121(3):1873–1889, Mar. 2016. doi: 10.1002/2015jb012768.

McNamara, A. K. A review of large low shear velocity provinces and ultra low velocity zones. *Tectonophysics*, 760:199–220, June 2019. doi: 10.1016/j.tecto.2018.04.015.

Müller, G. The reflectivity method: a tutorial. *Journal of Geophysics*, 58(1):153–174, 1985.

Pisconti, A., Thomas, C., and Wookey, J. Discriminating Between Causes of D" Anisotropy Using Reflections and Splitting Measurements for a Single Path. *Journal of Geophysical Research: Solid Earth*, 124(5):4811–4830, May 2019. doi: 10.1029/2018jb016993.

Pisconti, A., Creasy, N., Wookey, J., Long, M. D., and Thomas, C. Mineralogy, fabric and deformation domains in D" across the southwestern border of the African LLSVP. *Geophysical Journal International*, 232(1):705–724, Sept. 2022. doi: 10.1093/gji/ggac359.

Rao, P. B., Ravi Kumar, M., and Singh, A. Anisotropy in the lowermost mantle beneath the Indian Ocean Geoid Low from ScS splitting measurements. *Geochemistry, Geophysics, Geosystems*, 18(2):558–570, Feb. 2017. doi: 10.1002/2016gc006604.

Reasoner, C. and Revenaugh, J. Short-period P wave constraints on D" reflectivity. *Journal of Geophysical Research: Solid Earth*, 104(B1):955–961, Jan. 1999. doi: 10.1029/1998jb900053.

Reiss, A., Thomas, C., van Driel, J., and Heyn, B. A hot midmantle anomaly in the area of the Indian Ocean Geoid Low. *Geophysical Research Letters*, 44(13):6702–6711, July 2017. doi: 10.1002/2017gl073440.

Ringler, A. T., Anthony, R. E., Aster, R. C., Ammon, C. J., Arrowsmith, S., Benz, H., Ebeling, C., Frassetto, A., Kim, W., Koelemeijer, P., Lau, H. C. P., Lekić, V., Montagner, J. P., Richards, P. G., Schaff, D. P., Vallée, M., and Yeck, W. Achievements and Prospects of Global Broadband Seismographic Networks After 30 Years of Continuous Geophysical Observations. *Reviews of Geophysics*, 60(3), Sept. 2022. doi: 10.1029/2021rg000749.

Ritsema, J., Deuss, A., van Heijst, H. J., and Woodhouse, J. H. S40RTS: a degree-40 shear-velocity model for the mantle from new Rayleigh wave dispersion, teleseismic travel time and normal-mode splitting function measurements. *Geophysical Journal International*, 184(3):1223–1236, Dec. 2010. doi: 10.1111/j.1365-246x.2010.04884.x.

Romanowicz, B., Cara, M., Fel, J. F., and Rouland, D. GEOSCOPE: A French initiative in long-period three-component global seismic networks. *Eos, Transactions American Geophysical Union*, 65(42):753–753, Oct. 1984. doi: 10.1029/eo065i042p00753-01.

Rost, S. and Thomas, C. ARRAY SEISMOLOGY: METHODS AND APPLICATIONS. *Reviews of Geophysics*, 40(3), Sept. 2002. doi: 10.1029/2000rg000100.

Rost, S. and Thomas, C. Improving Seismic Resolution Through Array Processing Techniques. *Surveys in Geophysics*, 30(4–5): 271–299, May 2009. doi: 10.1007/s10712-009-9070-6.

Roult, G., Montagner, J. P., Romanowicz, B., Cara, M., Rouland, D., Pillet, R., Karczewski, J. F., Rivera, L., Stutzmann, E., and Maggi, A. The GEOSCOPE Program: Progress and Challenges during the Past 30 Years. *Seismological Research Letters*, 81(3):427–452, May 2010. doi: 10.1785/gssrl.81.3.427.

Scherbaum, F., Krüger, F., and Weber, M. Double beam imaging: Mapping lower mantle heterogeneities using combinations of source and receiver arrays. *Journal of Geophysical Research: Solid Earth*, 102(B1):507–522, Jan. 1997. doi: 10.1029/96jb03115.

Schweitzer, J., Fyen, J., Mykkeltveit, S., and Kvaerna, T. 9. Seismic Arrays. In *New Manual of Seismological Observatory Practice (NMSOP)*, Bormann, P., editor, pages 1–52. Deutsches GeoForschungsZentrum GFZ, 2009. doi: 10.2312/GFZ.NMSOP_R1_CH9.

Shephard, G. E., Matthews, K. J., Hosseini, K., and Domeier, M.

On the consistency of seismically imaged lower mantle slabs. *Scientific Reports*, 7(1), Sept. 2017. doi: 10.1038/s41598-017-11039-w.

Simmons, N. A., Myers, S. C., Johannesson, G., Matzel, E., and Grand, S. P. Evidence for long-lived subduction of an ancient tectonic plate beneath the southern Indian Ocean. *Geophysical Research Letters*, 42(21):9270–9278, Nov. 2015. doi: 10.1002/2015gl066237.

Spasojevic, S., Gurnis, M., and Sutherland, R. Mantle upwellings above slab graveyards linked to the global geoid lows. *Nature Geoscience*, 3(6):435–438, May 2010. doi: 10.1038/ngeo855.

Stähler, S. C., Khan, A., Banerdt, W. B., Lognonné, P., Giardini, D., Ceylan, S., Drilleau, M., Duran, A. C., Garcia, R. F., Huang, Q., Kim, D., Lekic, V., Samuel, H., Schimmel, M., Schmerr, N., Sollberger, D., Stutzmann, E., Xu, Z., Antonangeli, D., Charalambous, C., Davis, P. M., Irving, J. C. E., Kawamura, T., Knapmeyer, M., Maguire, R., Marusiak, A. G., Panning, M. P., Perrin, C., Plesa, A.-C., Rivoldini, A., Schmelzbach, C., Zenhäusern, G., Beucler, E., Clinton, J., Dahmen, N., van Driel, M., Gudkova, T., Horleston, A., Pike, W. T., Plasman, M., and Smrekar, S. E. Seismic detection of the martian core. *Science*, 373(6553):443–448, July 2021. doi: 10.1126/science.abi7730.

Stammler, K. Seismichandler—Programmable multichannel data handler for interactive and automatic processing of seismological analyses. *Computers & Geosciences*, 19(2):135–140, Feb. 1993. doi: 10.1016/0098-3004(93)90110-q.

Thomas, C. and Weber, M. P velocity heterogeneities in the lower mantle determined with the German Regional Seismic Network: improvement of previous models and results of 2D modelling. *Physics of the Earth and Planetary Interiors*, 101(1–2):105–117, Apr. 1997. doi: 10.1016/s0031-9201(96)03245-1.

Thomas, C., Weber, M., Wicks, C. W., and Scherbaum, F. Small scatterers in the lower mantle observed at German broadband arrays. *Journal of Geophysical Research: Solid Earth*, 104(B7): 15073–15088, July 1999. doi: 10.1029/1999jb900128.

Thomas, C., Kendall, J.-M., and Weber, M. The lowermost mantle beneath northern Asia-I. Multi-azimuth studies of a D″ heterogeneity. *Geophysical Journal International*, 151(1):279–295, Oct. 2002. doi: 10.1046/j.1365-246x.2002.01759.x.

Thomas, C., Garnero, E. J., and Lay, T. High-resolution imaging of lowermost mantle structure under the Cocos plate. *Journal of Geophysical Research: Solid Earth*, 109(B8), Aug. 2004a. doi: 10.1029/2004jb003013.

Thomas, C., Kendall, J.-M., and Lowman, J. Lower-mantle seismic discontinuities and the thermal morphology of subducted slabs. *Earth and Planetary Science Letters*, 225(1–2):105–113, Aug. 2004b. doi: 10.1016/j.epsl.2004.05.038.

Thomas, C., Wookey, J., Brodholt, J., and Fieseler, T. Anisotropy as cause for polarity reversals of D″ reflections. *Earth and Planetary Science Letters*, 307(3–4):369–376, July 2011. doi: 10.1016/j.epsl.2011.05.011.

Tsekhmistrenko, M., Sigloch, K., Hosseini, K., and Barruol, G. A tree of Indo-African mantle plumes imaged by seismic tomography. *Nature Geoscience*, 14(8):612–619, June 2021. doi: 10.1038/s41561-021-00762-9.

Usui, Y., Hiramatsu, Y., Furumoto, M., and Kanao, M. Evidence of seismic anisotropy and a lower temperature condition in the D″ layer beneath Pacific Antarctic Ridge in the Antarctic Ocean. *Physics of the Earth and Planetary Interiors*, 167(3–4):205–216, Apr. 2008. doi: 10.1016/j.pepi.2008.04.006.

Weber, M. P- and S-wave reflections from anomalies in the lowermost mantle. *Geophysical Journal International*, 115(1): 183–210, Oct. 1993. doi: 10.1111/j.1365-246x.1993.tb05598.x.

Weber, M. and Davis, J. P. Evidence of a laterally variable lower mantle structure from P- and S-waves. *Geophysical Journal International*, 102(1):231–255, July 1990. doi: 10.1111/j.1365-246x.1990.tb00544.x.

Weber, M. and Körnig, M. A search for anomalies in the lowermost mantle using seismic bulletins. *Physics of the Earth and Planetary Interiors*, 73(1–2):1–28, Sept. 1992. doi: 10.1016/0031-9201(92)90104-4.

Wessel, P. and Smith, W. H. F. New version of the generic mapping tools. *Eos, Transactions American Geophysical Union*, 76 (33):329–329, Aug. 1995. doi: 10.1029/95eo00198.

Wolf, J., Long, M. D., Li, M., and Garnero, E. Global Compilation of Deep Mantle Anisotropy Observations and Possible Correlation With Low Velocity Provinces. *Geochemistry, Geophysics, Geosystems*, 24(10), Oct. 2023. doi: 10.1029/2023gc011070.

Wookey, J., Stackhouse, S., Kendall, J.-M., Brodholt, J., and Price, G. D. Efficacy of the post-perovskite phase as an explanation for lowermost-mantle seismic properties. *Nature*, 438(7070): 1004–1007, Dec. 2005. doi: 10.1038/nature04345.

Wright, C. and Kuo, B.-Y. The P-wavespeed structure in the lowermost 700km of the mantle below the central part of the Indian Ocean. *Physics of the Earth and Planetary Interiors*, 161(3–4): 243–266, May 2007. doi: 10.1016/j.pepi.2007.02.006.

Wright, C., Muirhead, K. J., and Dixon, A. E. The P wave velocity structure near the base of the mantle. *Journal of Geophysical Research: Solid Earth*, 90(B1):623–634, Jan. 1985. doi: 10.1029/jb090ib01p00623.

Wysession, M. E., Lay, T., Revenaugh, J., Williams, Q., Garnero, E. J., Jeanloz, R., and Kellogg, L. H. *The D″ discontinuity and its implications*, page 273–297. American Geophysical Union, 1998. doi: 10.1029/gd028p0273.

Yamada, A. and Nakanishi, I. Detection of P-wave reflector in D″ beneath the south-western Pacific using double-array stacking. *Geophysical Research Letters*, 23(13):1553–1556, June 1996. doi: 10.1029/96gl01564.

Yamada, A. and Nakanishi, I. Short-wavelength lateral variation of a D′′ P-wave reflector beneath the southwestern Pacific. *Geophysical Research Letters*, 25(24):4545–4548, Dec. 1998. doi: 10.1029/1998gl900188.

Young, C. J. and Lay, T. Evidence for a shear velocity discontinuity in the lower mantle beneath India and the Indian Ocean. *Physics of the Earth and Planetary Interiors*, 49(1–2):37–53, Nov. 1987. doi: 10.1016/0031-9201(87)90131-2.

Yu, S. and Garnero, E. J. Ultralow Velocity Zone Locations: A Global Assessment. *Geochemistry, Geophysics, Geosystems*, 19 (2):396–414, Feb. 2018. doi: 10.1002/2017gc007281.